Low sidelobe limited diffraction optical coherence tomography

Jian-yu Lu[*a], Jiqi Cheng[a], and Brent D. Cameron[b]

[a]Ultrasound Laboratory, University of Toledo; [b]Biomedical Optics Lab, University of Toledo

ABSTRACT

Optical Coherence Tomography (OCT) is a relatively new type of imaging system for medical diagnosis. Because most current OCT systems use a sharply focused beam in tissues, they have a short depth of field (high image resolution is near the focus only). In this paper, limited diffraction beams of different orders are used to increase depth of field and to reduce sidelobes in OCT. Results show that the proposed OCT system has a lateral resolution of about 4.4 wavelengths (the central wavelength of the source is about 940 nm with a bandwidth of about 70 nm) and lower than -60 dB sidelobes over an entire depth of field of 4.5 mm with the diameter of the objective lens of 1 mm.

Keywords: Limited diffraction beams, optical coherence tomography, sidelobe reduction

1. INTRODUCTION

Optical Coherence Tomography (OCT) is a relatively new noninvasive optical imaging modality for biomedical diagnosis. It is based on low-coherence reflectometry[1], which was first developed for measuring telecommunication devices of a high precision in the range of micrometers and later introduced to biomedical areas as a method to map the contour and monitor the thickness of retina[2]. Huang et al[3] further extended this principle to get two-dimensional images by scanning the probe arm or testing object in the lateral direction. Since OCT has a much higher spatial resolution compared to other imaging modalities, such as X-ray CT, MRI, and high-resolution ultrasound, it has significant potential in medical diagnosis. Its applications in ophthalmology, dermatology, endoscopy, cardiology, vascular morphology, gastroenterology, dentistry, and embryology have been demonstrated by several research groups[3-7].

In principle, OCT works in a way very similar to B-scan ultrasound. It detects the back-scattered light from an object, while B-scan ultrasound detects back-scattered sound waves. Since the velocity of light is extremely high and the coherent time of the light source is very short, to detect the light pulse directly is very difficult. Instead, Michelson interferometer is used to detect the interference between the recombined electric fields from the probe arm and the reference arm. The interference pattern defines the axial resolution of an OCT, which is related to the bandwidth of the light source. With ultra-fast lasers, the axial resolution of an OCT can reach 2-4 μm that is comparable to the resolution of a microscope, (about 1 μm[8]). Normally, the lateral resolution of an OCT is determined by the central wavelength of the light source and numerical aperture (NA) of the objective. For practical purposes, a depth of field of about 2-3 mm is desirable, however, to keep such a large depth of field an objective with a low NA must be used. Assuming a depth of field of about 2 mm, the theoretical lateral resolution at the focal plane will be about 35 times of the center wavelength[9] (assuming the wavelength is about 940 nm) and the average resolution over the entire imaging distance would be even worse. Furthermore, the energy efficiency will be low due a large *f*-number.

To improve the lateral resolution and increase the depth of field, a new method is proposed where limited diffraction beams instead of focused Gaussian beams are used to illuminate the object. Limited diffraction Bessel beams were first demonstrated optically by Durnin et al[10,11]. They were produced with a thin circular slit in the focal plane of a lens. These beams can propagate to a large distance without spreading in transverse direction (a large depth of field) while maintaining a beam width of a few wavelengths. The drawback with Durnin's implementation method is that the energy efficiency of the beams is very low. To increase efficiency, Uehara et al[12] developed an argon ion laser with a modified

[*] jilu@eng.utoledo.edu; phone 1 419 530-8079; 1 419 530-8076; http://bioe.eng.utoledo.edu; Ultrasound Laboratory, University of Toledo, 2801 W. Bancroft, Toledo, OH 43606

Coherence Domain Optical Methods in Biomedical Science and Clinical Applications VI, Valery V. Tuchin, Joseph A. Izatt, James G. Fujimoto, Editors, Proceedings of SPIE Vol. 4619 (2002) © 2002 SPIE · 1605-7422/02/$15.00

cavity capable of generating limited diffraction beams; Vasara et al[13] proposed another more simper way by using a laser and a single computer-generated hologram. With a four-level phase-only hologram, the efficiency can be as high as 81.5%. In addition, the intensity at the center of beams generated by a single hologram is increased linearly with the propagating distance within the depth of field. This is an obvious advantage when applied to OCT as compared to use Durnin's beams where the intensity at the beam center is relatively constant. The increased intensity will naturally compensate for the intensity decrease due to the attenuation of the light in tissue.

In previous studies, we have produced the limited diffraction beams with ultrasound[14-21] and applied them to medical imaging[22-26], tissue property identification[27], nondestructive evaluation[28], blood flow velocity measurement[29], and optical communications[30]. We also developed methods to reduce sidelobes of limited diffraction beams, such as, inverse filtering[31], bowtie beams[32-33], and summation-subtraction[34]. With the summation-subtraction method, a high quality image can be obtained over a very large depth of field. In this paper, we have extended the method developed in ultrasound to OCT. In this method, the objective of the probe arm of an OCT is replaced with a limited diffraction beam transmitter and receiver while the basic structure of the Michelson interferometer remains the same. The proposed limited diffraction beam transmitter and receiver are implemented with a method similar to the hologram technique mentioned above. To generate a zero-order Bessel beam, a two-level phase-only mask is used. Higher-order diffraction, produced from the mask, is removed with an iris diaphragm and quadratic phases are compensated. Second-order Bessel beams are produced by adding a second mask immediately behind the first one to modulate both the amplitude and phase in the angular (azimuthal) direction. The second mask can be rotated by 45^o to produce a rotated second-order beam. To reduce sidelobes, at each scanning position, the three backscattered signals obtained from the two second-order and one first-order measurement are recombined by summing the second order beams and then subtracting the first-order beam. Although this procedure requires three operations as oppose to one operation in conventional OCT to obtain a single image line, with the current design, an average lateral resolution of 4.4 wavelengths over a depth of field of about 4.5 mm with a low sidelobe can be achieved. In the next section, we will briefly introduce the basic theory of sidelobe reduction for limited diffraction beams; In Section 3, the system design of the new method will be presented. Simulation results based on a single scattering model of the interaction between light and object will be given. Finally, we will present a brief discussion and a conclusion.

2. THEORY

The basic structure of an OCT system is a Michelson interferometer, as is shown in Fig. 1. According to Pan et al[35]

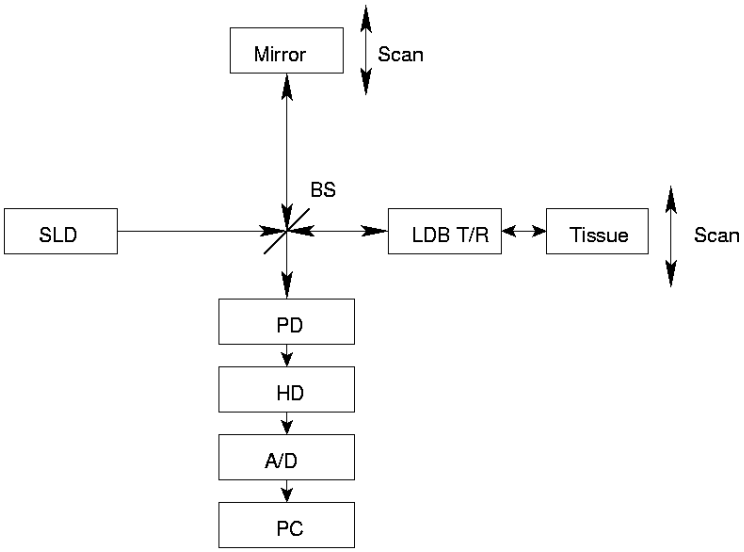

Fig. 1. Block diagram of OCT.
SLD: superluminescence diode, BS: beam splitter, LDB T/R: limited diffraction beams transmitter/receiver, PD: photodiode, HD: heterodyne detection, A/D: analog/digital converter, PC: personal computer

and ignoring the depolarization effects of the light, the detected signal for a fixed scanning position from one scatterer located at $\vec{r} = (r, \phi, z)$ can be expressed in terms of the axial distance as:

$$I_d(z'-z) = E_s E_s^* + E_r E_r^* + 2\left|E_s\right|\left|E_r\right|\left|V_{tc}(z'-z)\right|\cos\bar{k}(z'-z), \tag{1}$$

where E_s is the light field scattered from the tissue, E_r means the light field from the reference arm, and $z'-z$ is the optical distance difference between the reference and the probe arms, and $\bar{k}$ is the center wavenumber. The incoherent light is ignored in the above expression. The interference is given by the last term in (1). $V_{ct}(z)$ is the autocorrelation function of the light expressed in the space domain and is given by:

$$V_{tc}(z) = \exp(-\frac{z^2}{L_c^2}), \tag{2}$$

where L_c is the coherence length of the light source, which is related to the group velocity index of the object and the bandwidth, center wavelength of the light source, and is given by:

$$L_c = \left(\frac{2\sqrt{\ln 2}}{\pi}\right)\left(\frac{\bar{\lambda}^2}{n\Delta\lambda}\right). \tag{3}$$

L_c is directly related the axial resolution of OCT, which is $2\sqrt{\ln 2}L_c$ in our definition. After filtering out the direct current (DC) component and keeping the reference light filed constant, we have:

$$I(z'-z) \propto \left|E_s\right|\exp(-\frac{(z'-z)^2}{L_c^2})\cos(\bar{k}(z'-z)). \tag{4}$$

In conventional OCT, a focused Gaussian beam is used to illuminate the object. Its transverse sidelobes at the focal plane are very low, however, the depth of field is also very small. In our case, a limited diffraction beam, which has a very large depth of field, but higher sidelobes, is used to illuminate the object. To reduce the sidelobes, multiple limited diffraction beams are used. The rigorous theory and derivation has been discussed in a previous paper[34]. In the following, we give only major results. Using Bessel beams as an example, the field produced at the scatterer by a broadband Bessel light beams can be expressed as:

$$\Phi_{J_m}(\vec{r},t) = 2\pi J_m(\alpha r)\cos m(\phi-\phi_0)F^{-1}\left\{T(\omega)e^{j\beta z}\right\}, \tag{5}$$

where $m = 0, 1, 2, \cdots$, is the order of the Bessel beams, α is the scaling parameter, ϕ_0 controls the starting angle of the beam, $\beta = \sqrt{\bar{k}^2 - \alpha^2}$, and where $\bar{k}$ is the wavenumber. $T(\omega)$ is square root of spectrum distribution function of the light source. $F^{-1}(\bullet)$ represents the inverse Fourier transform. Because OCT is similar to a pulse-echo system, according to the reciprocal principle, the detected signal from the point scatterer located at $\vec{r} = (r, \phi, z)$ with reflection coefficient of $A(r, \phi, z)$ is given by:

$$e_{J_m}(\vec{r},t) = 4\pi^2 A(\vec{r})J_m^2(\alpha r)\cos^2 m(\phi-\phi_0)\bullet F^{-1}\left\{T(\omega)e^{j2\beta z}\right\}. \tag{6}$$

In the case of OCT, the last term in (6) is related to the interference term in (4). By rewriting (6) in space domain and substituting it into (4), we have:

$$I(z'-z) = 4\pi^2 A(\vec{r})J_m^2(\alpha r)\cos^2 m(\phi-\phi_0)\bullet\exp(-\frac{(z'-z)^2}{L_c^2})\cos(\bar{k}(z'-z)). \tag{7}$$

In a linear system, the total detected signal is the sum of contributions from all scatterers illuminated. By integrating over above equation, we obtain an A-line:

$$I(z'-z) = 4\pi^2\int_{-\infty}^{\infty} r dr\int_{-\pi}^{\pi} d\phi\int_{-\infty}^{\infty} dz\ \cdot\left[A(\vec{r})J_m^2(\alpha r)\cos^2 m(\phi-\phi_0)\bullet\exp(-\frac{(z'-z)^2}{L_c^2})\cos(\bar{k}(z'-z))\right]. \tag{8}$$

Because $J_0^2(0)=1$ and $J_2^2(0)=0$, and $J_0^2(\alpha r)\approx J_2^2(\alpha r)\approx(2/\pi\alpha r)\cos^2(\alpha r-\pi/4)$ when $\alpha r\gg 1$, sidelobes can be greatly reduced by the summation-subtraction method where A-lines of both second-order transmissions are summed and then subtracted from the zero-order transmission. I.e.:

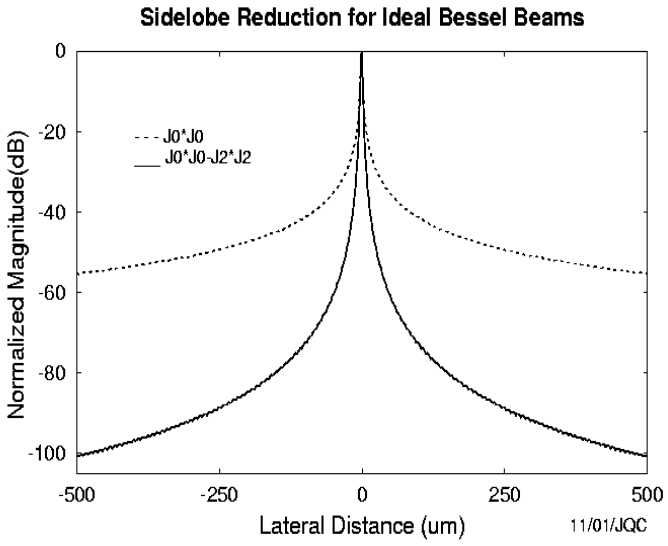

Fig.2. Sidelobe reduction for ideal Bessel beams

$$I_{J_0}(z')-[I_{J_2}(z')\big|_{\phi_0=0}+I_{J_2}(z')\big|_{\phi_0=\pi/4}]=4\pi^2\int_{-\infty}^{\infty}rdr\int_{-\pi}^{\pi}d\phi\int_{-\infty}^{\infty}dz\left[A(\vec{r})(J_0^2(\alpha r)-J_2^2(\alpha r))\cdot\exp(-\frac{(z'-z)^2}{L_c^2})\cos(\overline{k}(z'-z))\right]. \quad (9)$$

Assuming $\alpha=738151m^{-1}$ and the diameter of the aperture is $D=1mm$, the sidelobes are reduced by 40 dB at the edge of the aperture (see Fig. 2).

3. OPTICAL DESIGN

Our OCT system is the same as a conventional one except that the objective of the conventional OCT is replaced with the limited diffraction transmitter and receiver unit (Fig. 3). The unit uses masks to produce and receive limited diffraction beams. The designed depth of field of the limited diffraction Bessel beams is about 4.5 mm, and the full width

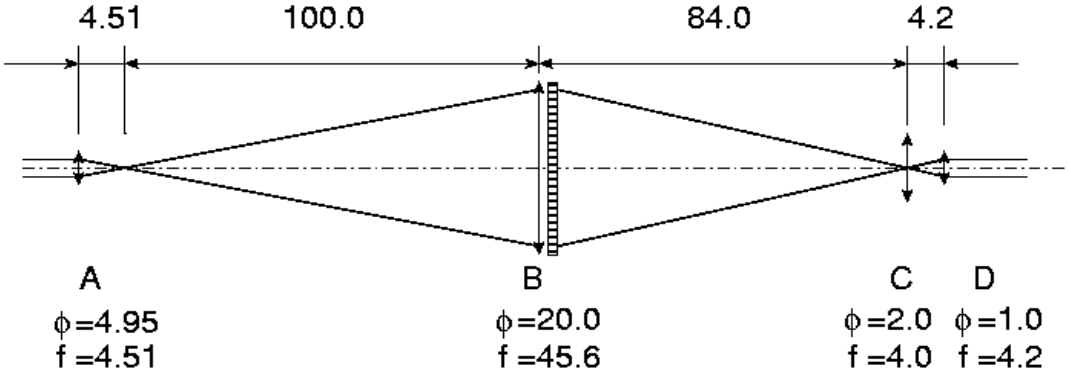

Fig.3. The diagram of the limited diffraction transmitter and receiver unit (Units are in mm)

at half maximum (FWHM) of the main lobe of the zero-order Bessel beam is approximately 4.4 center wavelengths. The center wavelength is about 940 nm, and the bandwidth is about 70 nm. The scaling parameter of the Bessel beams, α, is about 738151m^{-1}, and the diameter of the aperture is 1 mm. The phase function of the mask to produce the zero-order Bessel beam is given by[13]:

$$\Psi(r) = \alpha r - \pi / 4. \tag{10}$$

The field produced by such a phase mask is proportional to the axial distance from the mask[13]:

$$I(r, z) \propto z \left| J_0(\alpha r) \right|^2 . \tag{11}$$

For simplicity, the mask is implemented in two levels with the following phase function:

$$\Psi = \begin{cases} 0, & (\cos(\alpha' r - \pi / 4) \geq 0) \\ \pi, & (\cos(\alpha' r - \pi / 4) < 0) \end{cases}, \tag{12}$$

where $\alpha' = \alpha / 20$, is the scaling parameter of the mask (Fig. 4). In addition, the mask is 20 times larger than the designed aperture size facilitate manufacturing and handling. With these parameters, the mask has a total of 117 rings, with the width of each ring of about 85.1 μ m, except the first inner ring has a diameter of 127.7 μ m. The phase of each ring is either 0 or π as shown in Fig. 4. The diameter of the mask is 20 mm. As shown in Fig. 3, the light from the light source SLD passes through both lenses A and B. The lens B servers two purposes. First, it works with lens A to collimate the light; second, it provides a converging illumination for the masks. Lens C is an imaging lens that de-magnifies the mask by 20 times to produce the desired scaling parameter and aperture size for production of the Bessel beams. Lens D is used to cancel the quadratic phase introduced in the imaging process. According to Fourier optics[36], after the compensation of the quadratic phase, the resulting image is a convolution of the ideal image predicted by geometrical optics and the aperture of the imaging lens C. We have chosen the aperture of lens C so that it allows only the zero-order diffraction of the mask behind lens B to pass through. In theory, this contains about 40 percent of the total energy[13]. The magnitude of the light field immediately after the mask is unity, however, the image of the mask has a cosine transverse field profile due to the filtering effect. The field transverse profile calculated with linear convolution theory at lens D is shown in Fig. 5 (solid lines and dotted lines represent results before and after sidelobe reductions). To make it clear, in Fig. 5(a), only the maximum of each ring is plotted. The center 1/10 portion of the aperture is plotted in detail in Fig. 5(b) and the cosine-like pattern is clearly seen.

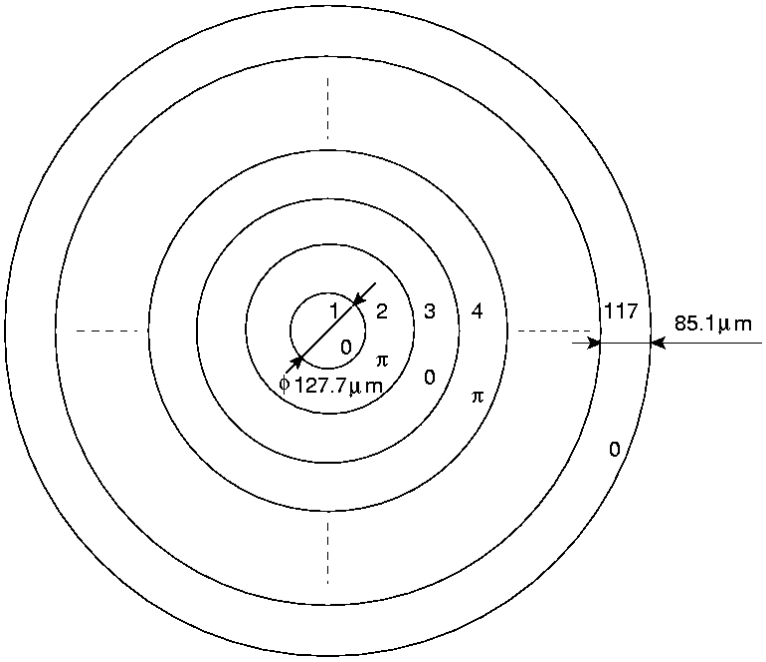

Fig.4. Diagram of the first mask

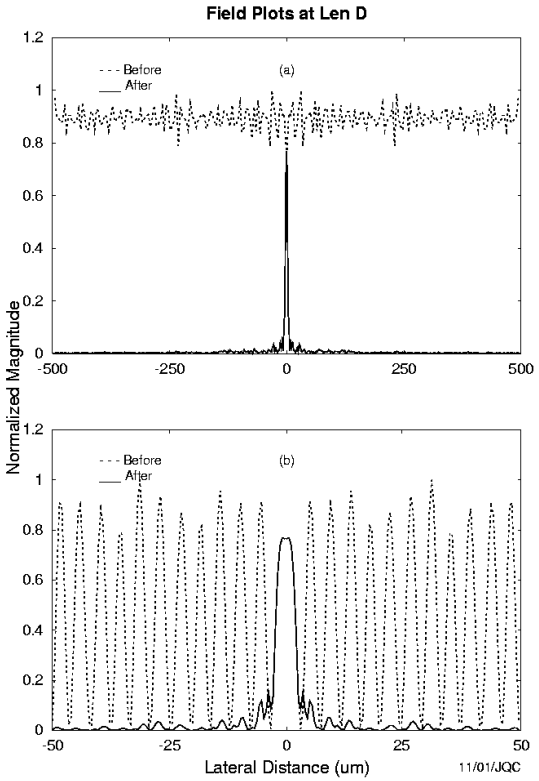

Fig.5. Field plots at lens D

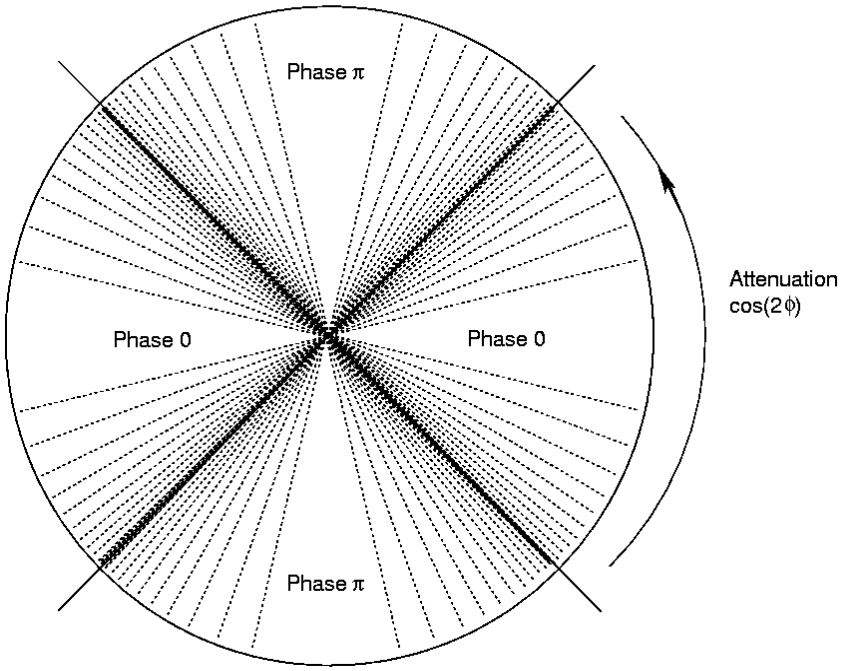

Fig.6. Diagram of the second mask

To generate the second order Bessel beams, a second mask is placed immediately behind the first at lens B. The

second mask modulates the phase and amplitude of the light in the angular (azimuthal) direction. A schematic of the second mask is shown in Fig. 6. It is divided into four quarters with an alternating phase of either 0 or π . The amplitude

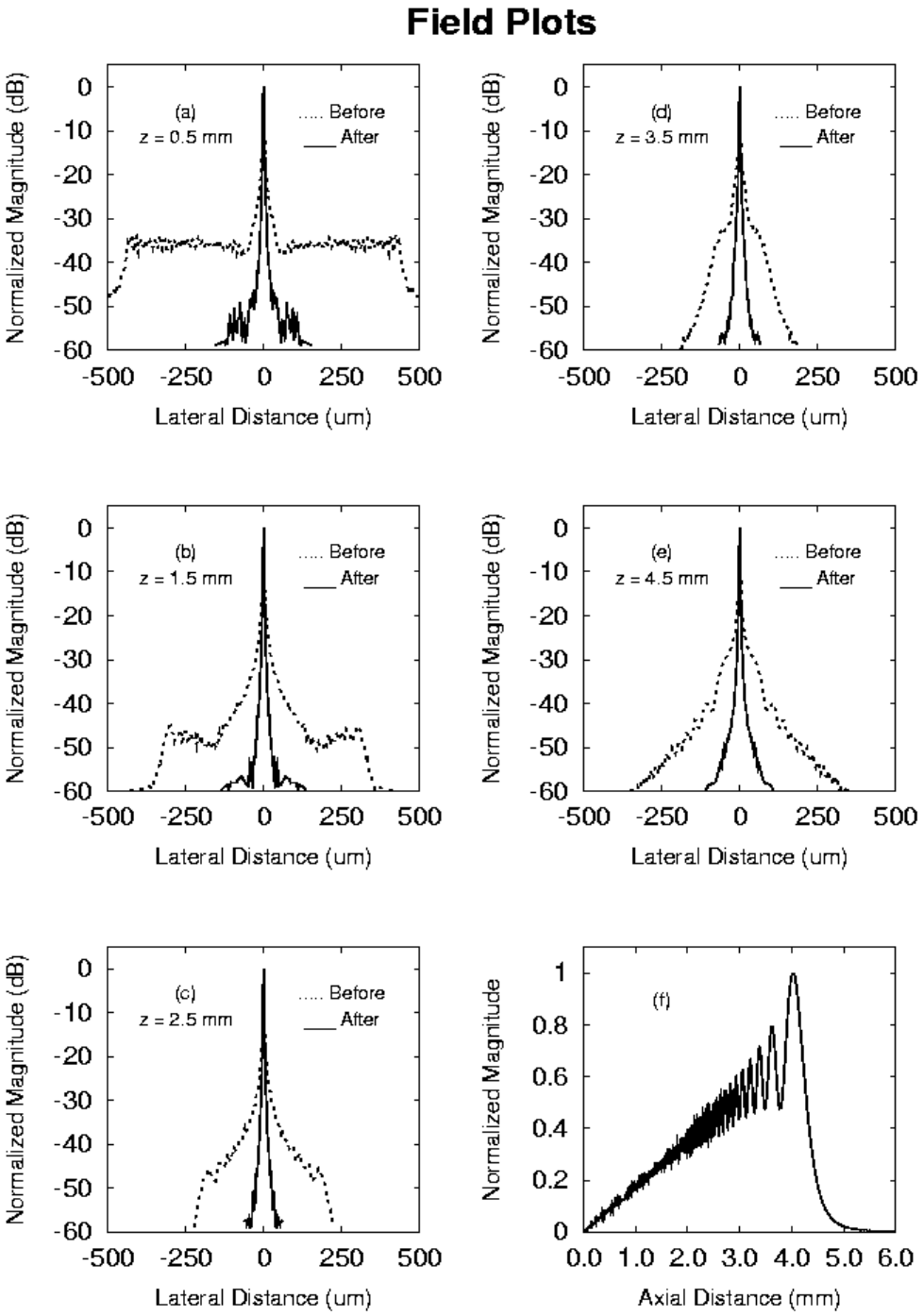

Fig.7. Field plots at different axial distances

transmission coefficient of the second mask is determined by the density of purely absorbing dots and is given by the function $\cos(2\phi)$. The second mask can be rotate 45 degree to produce the other second-order Bessel beam.

4. SIMULATION RESULTS

After passing through lens D, the light fields at five axial distances (0.5 mm, 1.5 mm, 2.5 mm, 3.5 mm, and 4.5 mm) are calculated with field calculation method developed by Ocheltree et al[37] (Fig. 7). The solid and dotted lines represent the results after and before the sidelobe reduction with the summation-subtraction method. It should be noted that even before sidelobe reduction, the Bessel beams have already kept their shapes without spreading in transverse direction over the display distances from 0.5-4.5 mm. After sidelobe reduction, the beams are nearly pencil beams over all depths from 0.0-4.5 mm (see both Figs. 5 and 7). Fig. 7(f) shows the increase of intensity of the zero-order Bessel beam with propagating distance within the depth of field, which agrees well with (11).

Computer simulation is also performed to verify the effect of the sidelobe reduction on a three-dimensional (3D) phantom containing multiple scatterers. The simulation is based on single scattering model, and (8) is used to calculate the detected signal. The constructed 2D images are shown in Fig. 8. The dimension of phantom is $240\times120\times120\mu m^3$, with two cylinders embedded. The diameters of these cylinders are 30μm and the reflection coefficients of the cylinders are 15 dB (Cyl. 1), -15 dB (Cyl. 2) relative to that of the bulk scattering background. In each cubic wavelength, one random scatter is assumed resulting in a total of over two million scatterers in the phantom. To show the limited diffraction property of the Bessel beams, images are simulated at five axial distances, where center of the phantom is place 0.5 mm, 1.5 mm, 2.5 mm, 3.5 mm and 4.5 mm away from the surface of lens D, respectively. A center wavelength of 940 nm with a bandwidth of 70 nm for the light source is assumed. The group velocity index of the phantom is taken as 1.37.

Constructed images of the phantom are shown in Figs. 9 and 10 before and after the summation-subtraction sidelobe

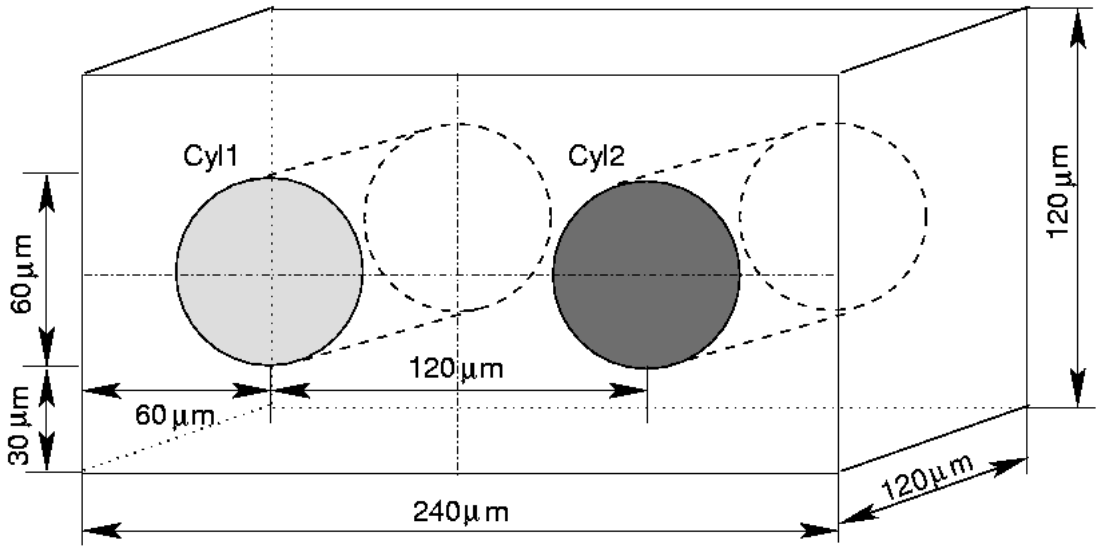

Fig. 8. Diagram of the phantom used for simulation

reduction. To avoid the influence of the edges, the images displayed are cut to $240\times100\mu m^2$. For comparison purposes, images are constructed at an axial distance of 2.5 mm with ideal Bessel beams are shown in both Figs. 9(f) and 10(f). It is clearly seen that the simplified masks produce satisfactory results as compared to ideal Bessel masks that are difficult to construct. We also see that the summation-subtraction method is effective for sidelobe reduction.

To quantitatively evaluate the image contrast, we use the following contrast definition:

$$contr = 20\log\frac{m_i}{m_o}, \tag{13}$$

where, m_i and m_o are the mean of the constructed image of the cylinder and the mean of background, respectively. To

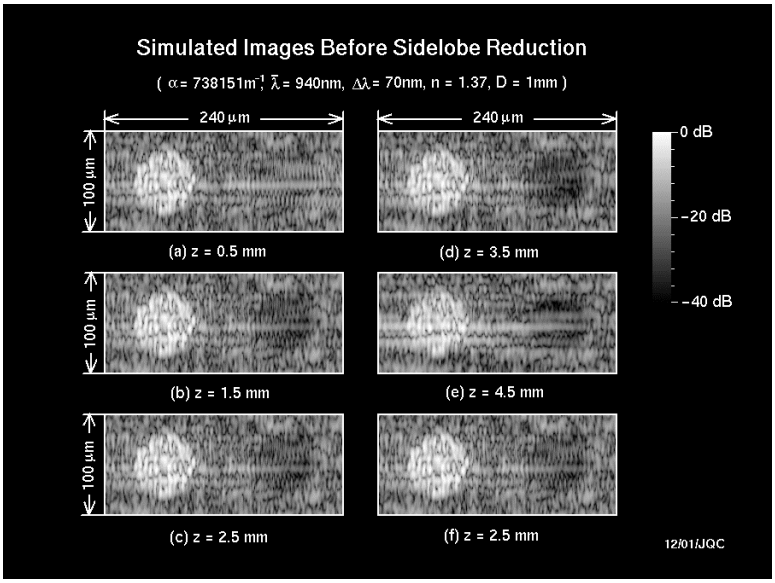

Fig. 9. Simulated images before sidelobe reduction

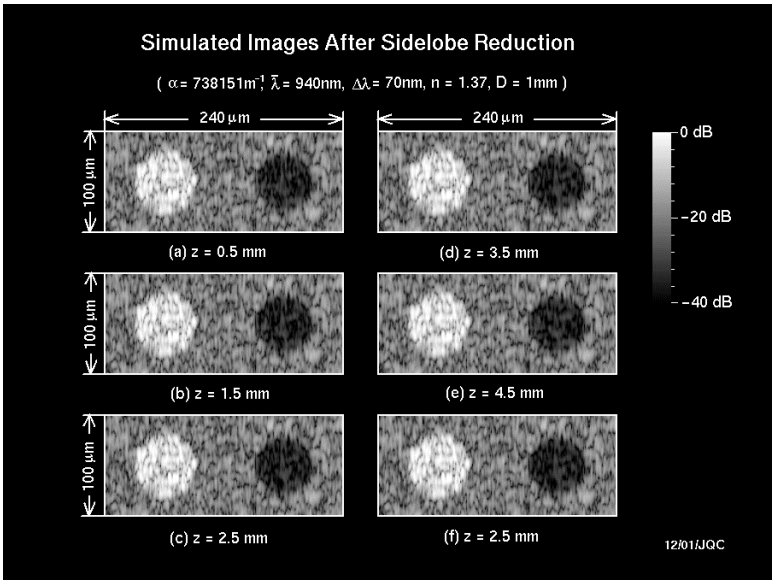

Fig. 10. Simulated images after sidelobe reduction

avoid the influence of the edges of the cylinders on the contrast, m_i and m_o are calculated with a radius of 4 μm smaller and larger than that of the cylinders, respectively. Calculated contrasts for all panels ((a)-(f)) in both Figs. 9 and 10 are listed in Table 1.

Table 1. Contrast of the cylinders in the phantom

	(a)		(b)		(c)		(d)		(e)		(f)	
	Cyl. 1	**Cyl. 2**	**Cyl. 1**	**Cyl. 2**	**Cyl. 1**	**Cyl. 2**	**Cyl. 1**	**Cyl. 2**	**Cyl. 1**	**Cyl. 2**	**Cyl. 1**	**Cyl. 2**
Ideal (dB)	15	-15	15	-15	15	-15	15	-15	15	-15	15	-15
Before (dB)	12.43	0.29	12.91	-6.01	12.86	-5.33	12.44	-7.91	12.31	-5.00	12.83	-5.04
After (dB)	14.94	-13.18	14.98	-13.66	14.96	-13.79	14.99	-13.57	14.91	-13.40	14.98	-13.91

5. DISCUSSION

5.1 Depth of field

The limited diffraction OCT system developed has a very large depth of field. In the current design, it is about 4.5 mm, which can be clearly seen from panel (f) of Fig. 7. At the surface of lens D, the beam has a high sidelobe before reduction (Fig. 5). From 0.5 mm to 4.5 mm, the beam has developed into a Bessel beam even without sidelobe reduction (Fig. 7). For biomedical applications, we are interested in about 2-3 mm in depth, therefore, the designed system is adequate for such applications (4.5 mm). Within the depth of field, image resolution is almost constant. This can also be seen from Figs. 9 and 10 where the speckle patterns of images at five axial distances have very similar features. In addition, within the depth of field, the intensity of Beams linearly increases with the propagating distance. This is clearly an advantage in the absorbing media such as biological soft tissues as it compensates for the attenuation.

5.2 Sidelobe

Compared to focused Gaussian beams at focal plane, limited diffraction beams have higher sidelobes. Fig. 2 shows the sidelobe levels for ideal zero-order Bessel beams. At the edge of the aperture, they are about –55dB. In the center of the Beams, the sidelobe level is so high that it is hard to construct images of a high contrast. However, with the summation-subtraction method, sidelobe is reduced to about –100dB at edge, and quickly reaches –60dB near the center. With our current implementation, at an axial distance of 0.5 mm, the sidelobe level before summation-subtraction is higher than the ideal beams, but at other depths, the actual sidelobes are lower. After summation-subtraction, the sidelobes at all depths are dramatically reduced, while the width of main lobe keeps nearly constant within the depth of field. In Fig. 9, the images have a low contrast before the sidelobe reduction. Cyl. 1 (–15dB) in Fig. 9 is hard to distinguish from the background. From Table 1, the actual contrast is only about –5dB to –8dB, which is well bellow the ideal –15dB. Furthermore at an axial distance of 0.5 mm, there is no contrast between this cylinder and the background. After the sidelobe reduction, the contrasts of the cylinders are very close to the ideal values – a high image contrast has been achieved.

5.3 Resolution

The axial resolution of our system is the same as that of the conventional OCT and is determined by the bandwidth and the center wavelength of the light source and group velocity index of the object. Since the wavelength around 800 nm is the window for biomedical optical applications where a good compromise between absorption and scattering is reached, the only practical way to increase the axial resolution is to broaden the bandwidth of light source. Through the use of ultra-fast laser pulses with a width in the range of a few femtoseconds, 1 μm axial resolution is achievable. However, the cost of such a light source may be extremely high. In most OCT systems, superluminescent diodes are used as the light source based on their low costs and reasonable performance. Generally, an axial resolution of 10 to 20 μm can be easily achieved. In a conventional system, there is a tradeoff between the lateral resolution and depth of field. If the sample is thin and placed near the focal zone, the lateral resolution can be very high, however, for a thicker sample, a low numerical aperture must be used to increase the depth of field thus leading to a low energy efficiency and low lateral resolution. The lateral resolution of our system is about 4.4 wavelenths, i.e. about 4 μm, and this resolution is maintained over 0-4.5 mm range after sidelobe reduction (Figs. 5 and 7). From Figs. 9 and 10, we can see that the lateral resolution is higher than that of the axial (8.13 μm) in the phantom images. Comparing panels (c) and (f) in both Figs. 9 and 10, it is clear that the simplified masks do not degrade beam performance and image quality.

5.4 Potential applications

A large depth of field and a high and constant lateral resolution are desirable for most OCT applications. In ophthalmology, it means a longer axial distance range can be imaged at a high and uniform resolution. In turbid media, the linearly increasing intensity of the light can naturally compensate for the attenuation to some degree. High and

constant lateral resolution also means less distortion of the image and high contrast between the interested features and the background, obviously, high contrast makes it easier to optically distinguish abnormal from normal tissues, which is very important for optical biopsy *in vivo*. Our current design provides a large depth of field and a high lateral resolution with low sidelobes. Currently, the masks need to be mechanical changed and rotated, thus the imaging time is at least three times longer and images are subject to motion artifacts. In the future, a liquid crystal spatial light modulator array could be used to quickly change the phase pattern electronically, thus reducing motion artifacts and to achieve the same demonstrated large depth of field and high resolution in a minimal increase in time compared to conventional OCT systems.

6. CONCLUSION

In this paper, a novel OCT system with a large depth of field, a high lateral resolution, and low sidelobes is developed based on limited diffraction beams and the summation-subtraction method. The main goal of this design is to overcome the problem of short depth of field of current OCT systems. An optical system and its masks are designed to produce and receive the limited diffraction Bessel beams. With the current design, the lateral and axial resolutions are about 4 μm and 8 μm over a large depth of field of about 4.5 mm, respectively. Simulations based on a single scattering model shows that within the depth of field, the current system can construct images with high contrast. Future studies will focus on the performance and physical implementation of the system under multiple scattering situations.

ACKNOWLEDGEMENTS

This work was supported in part by the grant HL60301 from the National Institutes of Health.

REFERENCES

1. B. L. Danielson and C. D. Whittenberg, "Guide-wave reflectometry with micrometer resolution," *Appl. Opt.* **26**, pp. 2836-2842, 1987.
2. G. S. Kino and S. S. C. Kim, "Mirau correlation microscope," *Appl. Opt.* **29**, pp. 3775-3783, 1990.
3. D. Huang, E. A. Swanson, C. P. Lin, J. S. Schuman, W. G. Stinson, W. Chang, M. R. Hee, T. Flotte, K. Gregory, C. A. Puliafito, and J. G. Fujimoto, "Optical coherence tomography," *Science*, **254**, pp. 1178-1181, 1991.
4. G. J. Tearney, M. E. Brezinski, B. E. Bouma, S. A. Boppart, C. Pitris, J. F. Southern, and J. G. Fujimoto, " In vivo endoscopic optical biopsy with optical coherence tomography," *Science*, **276**, pp. 2037-2039, 1997.
5. J. M. Schmitt, M. Yadlowsky, and R. F. Bonner, "Subsurface imaging of living skin with optical coherence microscopy," *Dermatology,* **191**, pp. 93-98, 1995.
6. Y. Pan and D. L. Farkas, "Noninvasive imaging of living human skin with dual-wavelength optical coherence tomography in two and three dimensions," *J. Biomed. Opt.* **3**, pp. 446-455, 1998.
7. B. W. Colston, Jr. U. S. Sathyam, L. B. DaSilva, M. J. Everett, P. Stroeve, and L. L. Otis, "Dental OCT," *Opt. Exp.* **3**, pp. 230-238, 1998.
8. D. A. Benaron, W. F. Cheong, D. K. Stevenson, "Tissue optics," Science, 276, pp. 2002-2003, 1997.
9. Jian-yu Lu, H. Zou, and J. F. Greeenleaf, "Biomedical ultrasound beam forming," *Ultrasound in Med. & Bio.*, **20**, pp. 403-428, 1994.
10. J. Durnin and J. J. Miceli, Jr., "Diffractin-Free Beams," *Phys. Rew. Lett.* **58**, pp. 1499-1501, 1987.
11. J. Drunin, "Exact solutions for nondiffracting beams. I. the scalar theory," *J. Opt. Soc. Am. A* **4**, pp 651-654, 1986.
12. K. Uehara and H. Kikuchi, "Generation of nearly diffraction-free laser beams," *Appl. Phys. B* **48**, pp. 125-129, 1989.
13. Vasara, J. Turumen, A. T. Friberg, "Realization of general nondiffracting beams with computer-generated holograms," *J. Opt. Soc. Am. A* **6**,1748-1754, 1989.
14. Jian-yu Lu and Anjun Liu, "An X wave transform," *IEEE Transactions on Ultrasonics, Ferroelectrics, and Frequency Control*, vol. **47**, no. 6, pp. 1472-1481, November, 2000.
15. Jian-yu Lu and J. F. Greenleaf, "Experimental verification of nondiffracting X waves," *IEEE Transactions on Ultrasonics, Ferroelectrics, and Frequency Control*, vol. **39**, no. 3, pp. 441-446, May, 1992.

16. Jian-yu Lu and J. F. Greenleaf, "Nondiffracting X waves - exact solutions to free-space scalar wave equation and their finite aperture realizations," *IEEE Transactions on Ultrasonics, Ferroelectrics, and Frequency Control*, vol. **39**, no. 1, pp. 19-31, January, 1992.
17. Jian-yu Lu, Hehong Zou and J. F. Greenleaf, "A new approach to obtain limited diffraction beams," *IEEE Transactions on Ultrasonics, Ferroelectrics, and Frequency Control*, vol. **42**, no. 5, pp. 850-853, September, 1995.
18. Jian-yu Lu, "Designing limited diffraction beams," *IEEE Transactions on Ultrasonics, Ferroelectrics, and Frequency Control*, vol. **44**, no. 1, pp. 181-193, January, 1997.
19. Jian-yu Lu, "Limited diffraction array beams," *International Journal of Imaging System and Technology*, vol. **8**, no. 1, pp. 126-136, January, 1997 (ISSN: 0899-9457).
20. Jian-yu Lu and J. F. Greenleaf, "A study of two-dimensional array transducers for limited diffraction beams," *IEEE Transactions on Ultrasonics, Ferroelectrics, and Frequency Control*, vol. **41**, no. 5, pp. 724-739, September, 1994.
21. Jian-yu Lu and J. F. Greenleaf, "Ultrasonic nondiffracting transducer for medical imaging," *IEEE Transactions on Ultrasonics, Ferroelectrics, and Frequency Control*, vol. **37**, no. 5, pp. 438-447, September, 1990.
22. Jian-yu Lu, "2D and 3D high frame rate imaging with limited diffraction beams," *IEEE Transactions on Ultrasonics, Ferroelectrics, and Frequency Control*, vol. **44**, no. 4, pp. 839-856, July, 1997.
23. Jian-yu Lu, "Experimental study of high frame rate imaging with limited diffraction beams," *IEEE Transactions on Ultrasonics, Ferroelectrics, and Frequency Control*, vol. **45**, no. 1, pp. 84-97, January, 1998.
24. Jian-yu Lu, Tai K. Song, Randall R. Kinnick, and J. F. Greenleaf, "In vitro and in vivo real-time imaging with ultrasonic limited diffraction beams," *IEEE Transactions on Medical Imaging*, vol. **12**, no. 4, pp. 819-829, December, 1993.
25. Jian-yu Lu and J. F. Greenleaf, "Pulse-echo imaging using a nondiffracting beam transducer," *Ultrasound in Medicine and Biology*, vol. 17, no. 3, pp. 265-281, May, 1991.
26. Jian-yu Lu and Shiping He, "Effects of phase aberration on high frame rate imaging," *Ultrasound in Medicine and Biology*, vol. **26**, no. 1, pp. 143-152, 2000.
27. Jian-yu Lu and J. F. Greenleaf, "Evaluation of a nondiffracting transducer for tissue characterization," in *IEEE 1990 Ultrasonics Symposium Proceedings*, 90CH2938-9, vol. **2**, pp. 795-798, 1990 (ISSN: 1051-0117).
28. Jian-yu Lu and J. F. Greenleaf, "Producing deep depth of field and depth-independent resolution in NDE with limited diffraction beams," *Ultrasonic Imaging*, vol. **15**, no. 2, pp. 134-149, April, 1993.
29. Jian-yu Lu, Xiao-Liang Xu, Hehong Zou, and J. F. Greenleaf, "Application of Bessel beam for Doppler velocity estimation," *IEEE Transactions on Ultrasonics, Ferroelectrics, and Frequency Control*, vol. **42**, no. 4, pp. 649-662, July, 1995.
30. Jian-yu Lu and Shiping He, "Optical X waves communications," *Optics Communications*, vol. **161**, pp. 187-192, March 15, 1999.
31. Jian-yu Lu and J. F. Greenleaf, "Diffraction-limited beams and their applications for ultrasonic imaging and tissue characterization," in *New Developments in Ultrasonic Transducers and Transducer Systems*, F. L. Lizzi, Editor, Proceedings SPIE, vol. **1733**, pp. 92-119, 1992 (ISBN: 0-8194-0906-5).
32. Jian-yu Lu, "Bowtie limited diffraction beams for low-sidelobe and large depth of field imaging," *IEEE Transactions on Ultrasonics, Ferroelectrics, and Frequency Control*, vol. **42**, no. 6, pp. 1050-1063, November, 1995.
33. Jian-yu Lu, "Producing bowtie limited diffraction beams with synthetic array experiment," *IEEE Transactions on Ultrasonics, Ferroelectrics, and Frequency Control*, vol. **43**, no. 5, pp. 893-900, September, 1996.
34. Jian-yu Lu and J. F. Greenleaf, "Sidelobe reduction for limited diffraction pulse-echo systems," *IEEE Transactions on Ultrasonics, Ferroelectrics, and Frequency Control*, vol. **40**, no. 6, pp. 735-746, November, 1993.
35. Y. Pan, R. Birngruber, J. Rosperich, and R. Engelhardt, “Low-coherence optical tomography in turbid tissue: theoretical analysis,” *Appl. Opt.* **34**, pp. 6564-6574, 1995.
36. J. W. Goodman, *Introduction to Fourier Optics*, chapt. 5, McGraw-Hill, New York., 1996.
37. K. B. Ocheltree and L. A.Frizzell, "Sound field calculation for rectangular sources," *IEEE Transactions on Ultrasonics, Ferroelectrics, and Frequency Control*, **36**, pp. 242-248, 1989.